Desalination and Water Treatment
www.deswater.com

doi: 10.5004/dwt.2022.28742

269 (2022) 188–199
September

Performance of zinc hydroxide coated activated carbon in the removal of methylene blue from aqueous solutions

Esra Altintig*, Simge Cabukcu

Sakarya University of Applied Sciences, Pamukova Vocational School, Sakarya 54900 Turkey, emails: altintig@subu.edu.tr (E. Altintig), simge_oncel@outlook.com (S. Cabukcu)

Received 2 March 2022; Accepted 16 July 2022

ABSTRACT

This study aimed to develop and characterize acorn shell-based activated carbon (AC) as a low-cost, abundantly available, highly efficient, and eco-friendly adsorbent. AC was modified ultrasonically using zinc hydroxide, $Zn(OH)_2$, and used effectively for the removal of methylene blue (MB) from aqueous solutions. MB is one of the most commonly used dyestuffs in the textile industry. The resulting products were characterized via analytical methods such as scanning electron microscopy, scanning electron microscopy/energy-dispersive X-ray spectroscopy, X-ray diffraction, and Fourier-transform infrared spectroscopy (SEM, SEM/EDS, XRD, and FTIR, respectively). The influence of different batch parameters, such as initial pH (3–10), adsorbent dosage (0.1–0.3 g/100 mL), temperature (298–318 K), initial dyestuff concentration (25–150 mg L^{-1}), and contact time (0–180 min), on the adsorption process, was examined. The highest maximum adsorption capacity was found to be 117.65 mg g^{-1} at 318 K from the Langmuir isotherm model for AC/$Zn(OH)_2$. The pseudo-second-order model determined the kinetics of MB dyestuff adsorption ($R^2 > 0.99$). According to the results of the thermodynamic parameters, standard negative values of Gibbs free energy, standard enthalpy, and standard entropy values were positive. These results revealed the endothermic nature of the adsorption process. After considering all the results, it was concluded that AC/$Zn(OH)_2$ adsorbent shows promise due to its manufacturability from a cheap source, high adsorption capacity, and short production time in addition to possessing eco-friendly characteristics, for removing MB dyestuff from aqueous solutions.

Keywords: Methylene blue; Activated carbon; synthesis; Ultrasonic support; Kinetic and isotherm

1. Introduction

Water pollution is one of the most important environmental problems in the world [1]. The leading visible water-polluting chemicals come from industries such as paints, textiles, leather, food processing, dyeing, pulp, and paper. Reactive dyes containing high-grade colored organic substances are used for coloring in the textile industry [2,3]. The dyestuffs found in textile wastewater are generally grouped in terms of being anionic, cationic, and non-ionic [2]. Dyes led to environmental and aesthetic problems by reducing the light transmittance in the receiving environment. In addition to these harmful effects, dyes accumulate in organisms and cause cancer formation [3,4]. Methylene blue (MB), a cationic dye from these groups, causes a decrease in biodiversity due to its toxicological and carcinogenic effects on living things, blocking the passage of sunlight, blocking the activities of aquatic plants, and being adsorbed by living microorganisms in the environment [4–6]. Various traditional chemical, physical and biological techniques have been used for the removal of dyestuffs from aqueous solutions such as ozonation [7], chemical oxidation [8], Fenton oxidation [9], ion exchange [10], advanced oxidation [11], and adsorption [12]. Among

* Corresponding author.

these methods, adsorption is recognized as an effective technology for water reuse due to its high level of efficiency, economic feasibility, low energy requirements, and efficient removal of toxic substances [13,14]. In the adsorption process, substances such as zeolite, wood ash, and activated carbons that are easy to produce are and suitable are used as adsorbents for decolorization [15]. Therefore, research has focused on the development of low-cost and effective adsorbents. One of these adsorbents, activated carbon, is a clearly defined, widespread, and versatile adsorbent that can be produced from carbon-containing substances such as biomass shells, lignin, and some polymers [16,17]. Its properties, including a large surface area, and convenient pore size, make activated carbon (AC) very different from other adsorbents [18]. ACs can be produced by physical activation, chemical activation or, a combination thereof [19]. Physical activation consists of carbonization and partial gasification with steam and CO_2 at high temperatures (700°C–1,000°C) [18]. Chemical activation, on the other hand, is carried out in one stage at a much lower temperature (450°C–700°C) in the presence of reagents such as H_3PO_4, KOH, NaOH, and $ZnCl_2$ [19–21]. Another reason why AC is used as an absorbent and is much preferred is that it can selectively retain organic and inorganic substances because of various functional groups created on its surface by various activation methods [22,23]. Various agricultural by-products such as hazelnut shells [24], rice shells [25], acorn shells [26], sour cherry stones [27], sugar cane waste [28], and sawdust [29] are widely used for low-cost AC production [25].

In recent years, researchers have increased the number of new adsorbent alternatives by combining ACs with other nanoparticles. For example, metal nanoparticles are produced by different methods [30,31]. Metal hydroxide nanoparticles are impregnated with activated carbon or other porous materials to enable the simultaneous removal of metal and organic contaminants [32,33]. These metal-based nanoparticles can also be regenerated by changing the pH of the solution and can be used even after several regenerations [34,35]. Researchers have tried different methods to modify these processes and adsorbents [32]. Some of these methods are in the form of thermal activation, acid cavitation, and acoustic cavitation. The basis of acoustic cavitation is the application of ultrasonic radiation to an aqueous medium. When the ultrasound spreads to the aqueous medium, cavitation bubbles are formed in the aqueous medium under the action of high ultrasonic pressure [36]. The bubbles so formed grow to an unstable size and settle inwards [32,36]. The acoustic cavitation mechanism can be used to enhance the activation of adsorbents and their adsorption capacity. The hydromechanical shear forces produced during cavitation deposition at a lower ultrasonic frequency are more intense since the bubbles formed at frequencies of 20 kHz or lower are relatively large in diameter [37].

In this study, the adsorption properties of low-cost AC produced from acorn bark against MB were investigated by modifying it with $Zn(OH)_2$ using the ultrasonic cavitation method. In the first stage of the study, activated carbons obtained from acorn shells were coated with $Zn(OH)_2$ using the ultrasonic cavitation method. The products so obtained were characterized by analytical methods such as scanning electron microscopy (SEM), scanning electron microscopy/energy-dispersive X-ray spectroscopy (SEM/EDS), X-ray diffraction (XRD), and Fourier-transform infrared spectroscopy (FTIR). The influence of different batch parameters such as the adsorbent dosage (0.1–0.3 g/100 mL), initial pH (3–10), temperature (298–318 K), initial MB concentration (25–150 mg L^{-1}), and contact time (0–180 min) on the adsorption process was investigated. Isotherm, kinetic and thermodynamic studies have been carried out to remove MB from aqueous solution. In addition, the maximum adsorption capacity of AC/$Zn(OH)_2$ has been determined.

2. Material and method

2.1. Material

The dye used in the study was methylene blue (MB) ($C_{16}H_{18}ClN_3S$) obtained from Merck (Darmstadt, Germany). The chemical structure of MB is shown in Fig. 1. HCl, zinc acetate, NaOH, and $ZnCl_2$ were obtained from Merck (Darmstadt, Germany). All chemical substances used in experiments are of analytical purity and have been used freshly prepared for experimental studies.

2.2. $Zn(OH)_2$ particles modified activated carbon

In the first stage of this work, AC was produced from acorn shells. For this purpose, acorn shells were collected from forests in the Sakarya region of Turkey. Firstly, the acorn shells were washed and air dried to remove the impurities contained in them. The crusts were then dried in an oven at 105°C for 24 h. They were then treated with $ZnCl_2$ with an impregnation ratio of 1:1. For carbonization, AC was placed in a tube oven at 700°C for 1 h. The AC was washed several times with distilled water until its filtrate was neutral. The typical synthesis of $Zn(OH)_2$/AC nanocomposites is described as follows: 9.17 g (0.05 mol) Zn $(CH_3COOH)_2$ was dissolved in 100 mL H_2O and (2 g) AC was added. The mixture was irradiated with ultrasound for 15 min, then 20 mL NaOH solution (2 M) was poured into the mixture and the white slurry so formed was irradiated with ultrasound for 20 kHz of ultrasonic frequency 120 W for 15 min at room temperature [38]. After the procedure was completed, the solution was filtered. To remove impurities from the mixture, ethanol, and water (50%) were washed with water and filtered

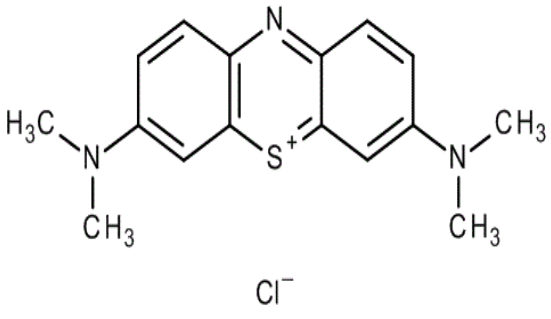

Fig. 1. Chemical structure of MB.

through a blue tape strainer. The resulting adsorbent was dried in an oven at 80°C for 12 h. After the drying process has been completed, the adsorbent was ground into powder and was ready for use.

2.3. Characterization

In the analysis of the synthesized adsorbents in the study, the SHIMADZU IR Prestige 21 unit FTIR spectrometer (Shimadzu Corp, Japan) (ATR method) was used to determine and clarify the absorbance values of the functional groups in their structure in the wavelength range of 4,000–400 cm^{-1}.

SEM analysis of the samples was performed using a Jeol JSM-6060 LV (Oxford Instruments, USA) to study the surface morphology and porosity. To observe the microporous structure of the surface, the samples were coated with a thin layer of gold and made conductive before scanning. The EDS analysis was displayed by focusing on a specific point in the scanned image area of the sample.

An X-ray diffractometer (Rigaku) branded XRD (Austin, USA) device was used in the qualitative structure analysis of the produced samples. The sample was analyzed at positions between 10° and 80° 2θ angle.

2.4. Adsorption procedure

The stock MB dyestuff solution was prepared with distilled water at a concentration of 1,000 mg L^{-1}. The desired concentrations were prepared by diluting a solution of this dyestuff. In adsorption experiments, the solution pH (3–10), contact time (5–100 min), the concentration of MB (25–150 mg L^{-1}), the effects of adsorbent dosage (0.1–1.0 g), and process temperature (298–318 K) parameters were determined separately. 1 M NaOH or 1 M HCl was used for pH adjustments. 0.1 g of adsorbent was added to the solutions and stirred for an h at 250 rpm in a shaker. After each time of contact, a sample was removed and centrifuged. The MB concentrations were determined using a Shimadzu Ultraviolet UV-Vis at 665 nm. The amount of MB adsorbed was derived from initial and final concentrations of MB in the liquid phases. All experiments were run in triplicate to ensure reproducibility.

The removal percentage (%) and the amount of MB in the adsorbent at equilibrium (q_e, mg g^{-1}) were determined using Eqs. (1) and (2), respectively [39].

$$q_e = \frac{\left(C_o - C_e\right)}{m} \times V \tag{1}$$

where C_o = ınitial MB concentration (mg L^{-1}), C_e = equilibrium MB concentration (mg L^{-1}), V = volume of solution (L), m = weight of the adsorbent (g).

$$\%\ \text{Removal} = \frac{\left(C_o - C_e\right)}{C_o} \times 100 \tag{2}$$

2.5. Determination of the point of zero charge (pHzpc)

The point of zero charges was determined as reported previously [17,18]. The procedure can be described as follows: to a series of 50 mL conical flasks, 30 mL of 0.1 M NaCl solution was added. The initial solution pH values of the NaCl solutions (initial pH) were adjusted in the range of 2–12 using 0.1 M HCl/NaOH solutions. After a constant value of initial pH was achieved, 0.1 g adsorbent (AC/$Zn(OH)_2$) was added to each conical flask which was capped immediately. These samples were shaken for 48 h, after which pH was measured for each sample (pH_f). Variations in the pH (pH = pH_f − pH_i) were plotted against the pH_i and the point of the intersection of the resulting curve at which pH = 0 was the pHzpc value.

3. Results and discussion

3.1. Characterization of results

To examine the surface morphology, the AC, AC/$Zn(OH)_2$ were subjected to SEM before and after the adsorption process. Fig. 2 shows the SEM images (1,000x magnification).

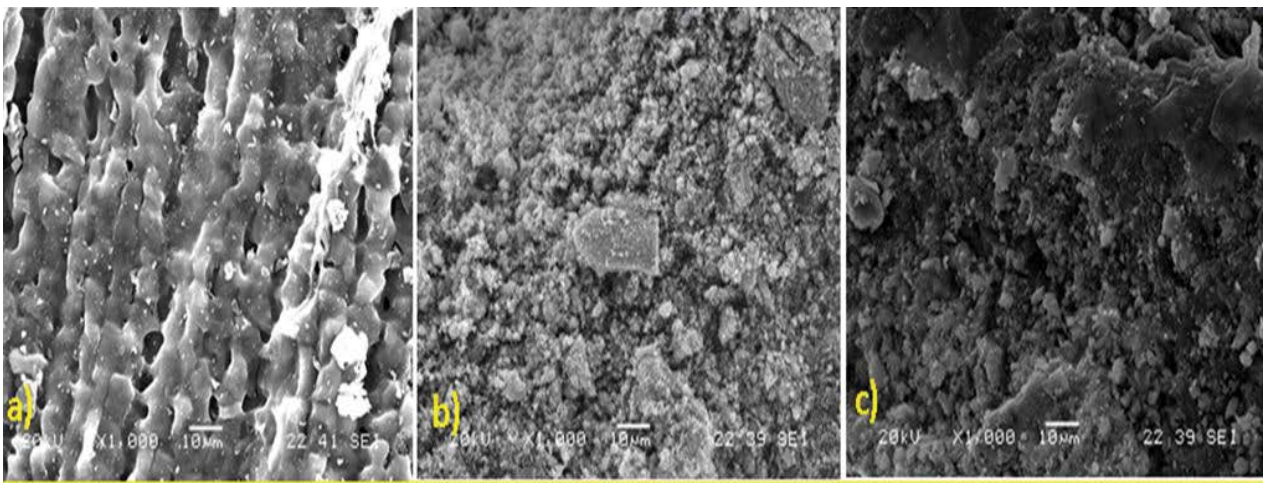

Fig. 2. SEM images of (a) AC, (b) AC/$Zn(OH)_2$ before adsorption of MB and (c) AC/$Zn(OH)_2$ after adsorption of MB.

Fig. 2a shows an SEM image of AC obtained from an acorn shell. When the SEM image is examined, gaps are seen on the surface. It is believed that the voids on this surface were previously filled by a chemical reagent, which caused the formation of such voids. These were visible on the surface of AC due to the evaporation of the chemical substance during carbonization [40]. It can be seen that the surface morphology of the voids seen on the surface of the activated carbon is homogeneous and relatively smooth.

In Fig. 2b the surface structure of AC is uniformly coated with $Zn(OH)_2$ nanoparticles. It has been observed that oxides of Zn were accumulated on the surface of AC. These clusters are irregular and form pores and cavities of different sizes on the surface.

Fig. 2c shows the SEM image after coating the AC/$Zn(OH)_2$ composite surface with MB dyestuff. From the photograph, it can be seen that the MB dyestuff was dispersed on the surface of the AC/$Zn(OH)_2$ composite. The observed darkness can be interpreted as MB adsorbed on the surface. Similar structures have been observed in $Zn(OH)_2$-NPs-AC obtained from a cherry tree composite for the adsorptive removal of MB from water [38].

Surface morphology, particle shape, and particle size according to the SEM images, and information about the element analysis according to EDS is given in Fig. 3.

As indicated in the EDS graph shown in Fig. 3a, the surface of the AC/$Zn(OH)_2$ sorbent is mainly composed of the elements C, O, and Zn obtained from the AC and $Zn(OH)_2$ sorbent.

EDS analysis was used to study the presence of elements forming $Zn(OH)_2$ nanoparticles, primarily zinc atoms, in the synthesized AC/$Zn(OH)_2$ nanocomposite. From the spectrum (Fig. 3b) corresponds to Zn, whose sharp peaks are observed at 1 and 9.6 keV.

Fig. 4 shows the results of FTIR analysis of AC, AC/$Zn(OH)_2$ before and after MB adsorption.

Evaluation of the functional groups of adsorbents and the verification of MB adsorption were inferred from FTIR spectra in Fig. 4. Fig. 4a gives the AC spectrum. AC does not have a distinct spectrum. The intensity of the peaks increased with the metal oxide modification. Metal oxides generally give an absorption band less than the wavenumber of 1,000 cm^{-1} due to their interatomic vibrations [41]. In Fig. 4b, the absorption peak of the wavenumber values of 800 and 430 cm^{-1} seen in the FTIR spectra extent to the Zn–O stress [38]. It is known that the peak acetate group with a wavenumber of 1,000 cm^{-1} corresponds to the C–O deformation mode. In our study, this peak corresponds to the wavenumber 1,175 cm^{-1}. The peak CH specified at 1,520 cm^{-1} corresponds to the vibrations of stretching and bending and out-of-plane bending of the components C=C and CH. The observed peak band with a wavenumber of 3,600 cm^{-1} is due to the O–H bonds of water, which, although small, remain on the surface of the crystals. Fig. 4c shows the FTIR spectrum after adsorption. Fig. 4b shows a decrease in intensities in the spectrum. After the adsorption of MB on the (AC/$Zn(OH)_2$) adsorbent, the peaks of the FTIR spectra (Fig. 4c) depicted a shift from their initial location and also a change in intensity, which verified the adsorption of MB by the adsorbent. The FTIR results revealed the introduction of various functional groups in the modification of $Zn(OH)_2$ to the AC surface. This can be useful in the adsorption process. It is so called because these surface functional groups can serve as "active sites".

The XRD patterns of the profiles of (a) AC, (b) AC/$Zn(OH)_2$, and (c) AC/$Zn(OH)_2$ after adsorption are shown in Fig. 5.

In Fig. 5a it is seen in the XRD spectrum that AC has a largely amorphous structure with a broad peak with a

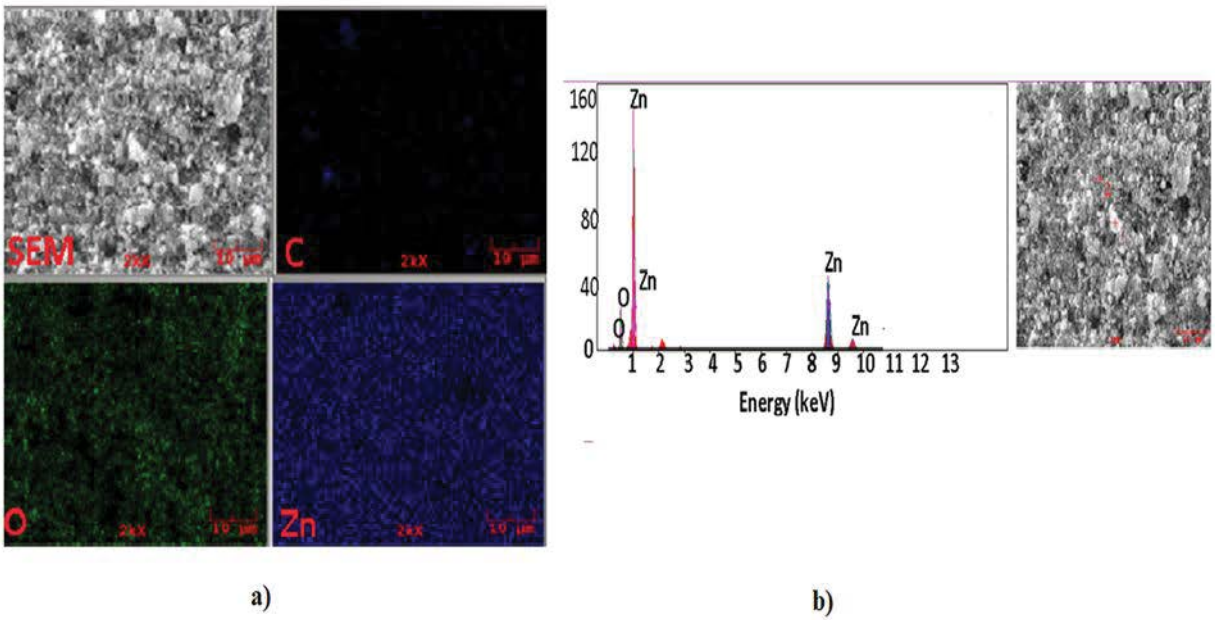

Fig. 3. (a) EDS mapping analysis area and the elemental mapping of (b) Zn, EDS point scan analysis area for the AC/$Zn(OH)_2$ composite.

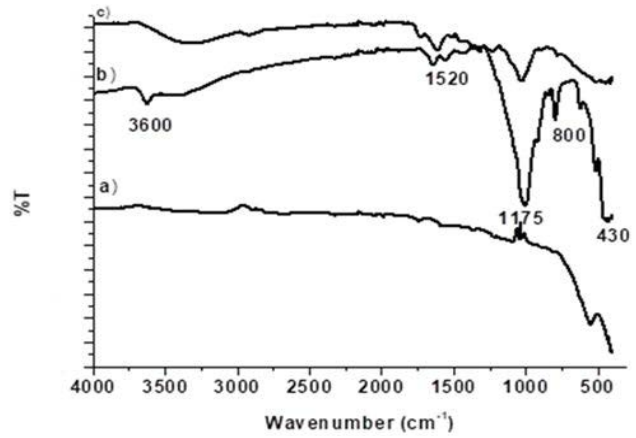

Fig. 4. FTIR of the spectrum of (a) AC, (b) AC/$Zn(OH)_2$ before adsorption of MB and (c) AC/$Zn(OH)_2$ after adsorption of MB.

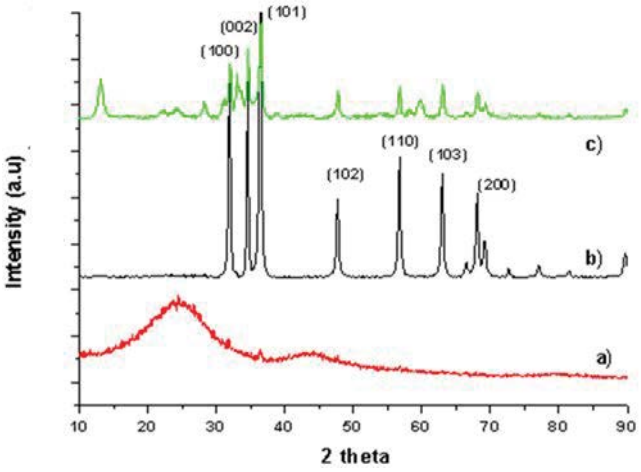

Fig. 5. XRD patterns of (a) AC, (b) AC/$Zn(OH)_2$ before adsorption of MB and (c) AC/$Zn(OH)_2$ after adsorption of MB.

maximum at 2θ = 25° [42,43]. There is similar to other studies in the literature [12,42,43]. When the XRD spectrum composites are examined in Fig. 5b, characteristic reflection 2θ peaks were seen at 31.75°, 35.02°, 37.27°, 49.86°, 57.55°, 63.45°, 69.59° and 70.02°. In the literature, these peaks are the specific peaks belonging to ZnO [31,38,41]. The powder XRD spectrum of AC/$Zn(OH)_2$ composites after MB adsorption were examined is shown in Fig. 5c, and the characteristic reflection of 2θ peaks are shown in the given. While these peaks formed before the adsorption of dyestuff are sharp, the sharpness formed after the adsorption of dyestuff decreases. This decrease indicates that the adsorption of MB has occurred.

3.2. Influence of initial pH

pH is one of the most important factors affecting adsorption. Since hydrogen (H^+) and hydroxyl (OH^-) ions are strongly adsorbed, the adsorption of other ions affects the pH of the solution [44]. pH affects not only the degree of ionization of adsorbates but also the surface charges of adsorbents. To investigate the pH effect of MB on $Zn(OH)_2$-coated AC, MB solutions with concentrations of 25 and 50 mg L^{-1} at varying initial pH values (3–10) were prepared. The data obtained regarding the effect of initial pH on MB adsorption and the change of adsorption with initial pH are shown in Fig. 6a. To find the optimum pH value, 0.1 g of AC/$Zn(OH)_2$ was added. MB solutions prepared at two different concentrations were mixed in a magnetic stirrer for 80 min. After centrifugation, the solid and liquid phases were separated, and the dyestuff was determined in the liquid phase using the UV spectroscopic method.

As shown in Fig. 6a, the removal efficiency of MB at both concentrations is observed to increase in this direction with an increase in the pH of the solution. The maximum adsorption of MB for both concentrations was at pH 7. This is thought to be due to a large amount of OH^- ions from NaOH present in the medium and the cationic structure of the dyestuff [45]. The adsorption of MB in cases where the pH is ≥5 at the concentration of MB is higher than the adsorption in an acidic pH environment. As seen in Fig. 6a, MB removal of 75%–71% at pH 3 to 6 and 91.17% at pH 7 was observed for 25 mg L^{-1} solutions. While the percentage of removal was 84.52 at pH 8, the removal decreased to 81.78% at pH 10. While the percentage removal efficiency for 50 mg L^{-1} MB solution was between 85.10%–94.63% at pH 3 to 6, the removal efficiency was determined as 95.97% at pH 7. The highest adsorption yields (91.17%–95.98%) for both initial concentrations were obtained at a pH value of 7. Therefore, pH 7.0 was chosen as the optimum pH value and used for all subsequent experiments. There are similar results for MB removal in the literature [43–45].

The pH_{PZC} is the point where the pH final–pH initial (ΔpH) versus the pH initial was zero. The results of pH_{PZC} for adsorbents can be seen in Fig. 6b. The pH_{PZC} for AC/$Zn(OH)_2$ is determined as pH 6.30. The positively charged surfaces of the activated carbon behave differently in the dye solution for ambient at pH < pH_{PZC} (pH at zero charges) while negatively charged surfaces are ambient pH > pH_{PZC}. The adsorption of cationic dyestuffs by AC/$Zn(OH)_2$ is more pronounced at pH > pH_{PZC}. On the other hand, anionic dyestuffs show a more pronounced adsorption behavior at pH < pH_{PZC}. Considering the adsorption between the negatively charged surface and the cationic dyestuff, the excess H^+ ions in the environment at acidic pH values settle in centers suitable for adsorption on the AC/$Zn(OH)_2$ and prevent the adsorption of cationic dyestuffs.

3.3. Influence of contact time

Contact time acts as one of the most effective adsorption parameters [45]. Three different adsorbent dosages (0.1–0.3 g) were used in the contact time (0–100 min) studies. To evaluate the adsorption characteristics of the AC/$Zn(OH)_2$ for MB, the change of adsorption rate with time has been investigated and revealed in Fig. 7.

The effect of AC/$Zn(OH)_2$ amount and time on the percentage of adsorptive that has been removed is shown in Fig. 7. For three different adsorbent doses, the percentage removal efficiency increased as the time increased.

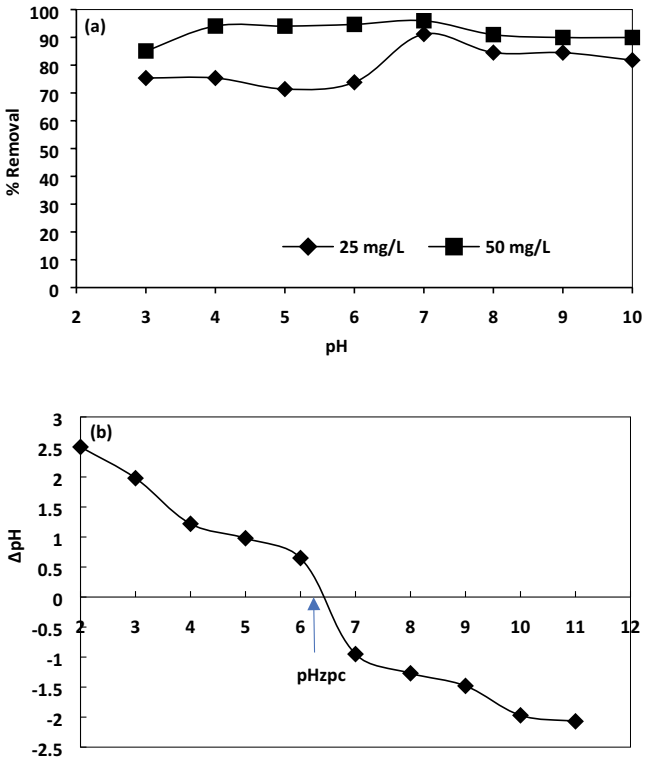

Fig. 6. (a) Effect of pH on MB (MB initial concentration: 25 vs. 50 mg L^{-1}; temperature: 298 K; contact time: 80 min, adsorbent dosage: 0.1 g L^{-1}) and (b) pH_{PZC} values of $AC/Zn(OH)_2$.

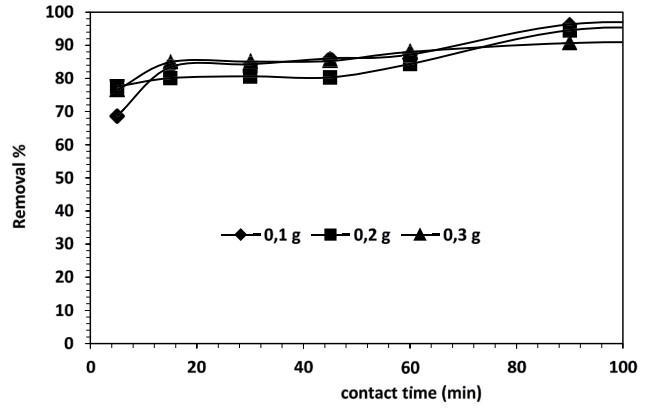

Fig. 7. Effect of contact time on the removal of MB by $AC/Zn(OH)_2$ (initial MB concentration: 50 mg L^{-1}; pH: 7; temperature: 298 K; adsorbent dosage: 0.1–0.3 g).

At a dose of 0.1 g adsorbent, the removal was 68% in the first 5 min but increased as time increased and reached 96.31% efficiency at the 80th min. At the 0.2 g adsorbent dose, the removal rate started at 77% in the first 5 min and increased to 94.55% in the 80th min. At a 0.3 g adsorbent dose, the yield started from 76.45% in the first 5 min and reached 90.65% in 80 min. The highest removal efficiency was reached at the 80th min in terms of the three different adsorbent doses. The optimum mixing time was determined as being 80 min. The contact time was continued for up to 100 min to determine the exact result. As the amount of adsorbent increased in terms of the three different doses, the percentage removal decreased. In addition, for three different adsorbent doses, the highest efficiency was achieved with a 0.1 g adsorbent dose for 80 contact min. Therefore, as in other studies, the optimum adsorbent dose was taken to be 0.1 g and a similar trend has been noted in many studies [46,47].

3.4. Adsorption isotherm models

Adsorption isotherm is very important. It can be used to describe how adsorbate interacts with adsorbents. The reaction mechanism of the adsorption system could be deduced by some theoretical or empirical models. The Langmuir and Freundlich isotherms were widely used to study the relationship between the adsorption capacity and the equilibrium concentration of adsorbate under a certain temperature [48]. For this purpose, using data obtained at different temperatures (298–318 K), how the adsorption changes were studied with the help of different isotherms (Langmuir and Freundlich isotherms). To determine the decisiveness of these obtained data with the isotherm model, it is necessary to reveal the relationship between equilibrium concentration and C_e/q_e. This relationship is explained by the equality and curve formation given in Fig. 8, and then isotherm constants are obtained from the slope and shear values of the curve. The linear form of the Langmuir [Eq. (3)] and Freundlich [Eq. (4)] equations are commonly given by:

Langmuir model:

$$\frac{C_e}{q_e} = \frac{1}{q_{\max} b} + \frac{C_e}{q_{\max}} \tag{3}$$

Freundlich model:

$$\ln q_e = \ln K_f + \frac{1}{n} C_e \tag{4}$$

where K_f and n refer to Freundlich's constants.

In these equations, q_e refers to the amount of MB adsorbed by the adsorbent (mg g^{-1}); C_e refers to the concentration of MB in equilibrium (mg L^{-1}). Where q_{max} is the monolayer adsorption capacity of the adsorbent (mg g^{-1}) and b is the Langmuir adsorption constant (L mg^{-1}), K_f and n refer to Freundlich's constants [48].

The isothermal adsorption process was conducted at the temperature of 298, 308, and 318 K. Fig. 8 depicts that the $AC/Zn(OH)_2$ adsorption capacity increased with the initial MB concentration and the experimental temperature, revealing that the adsorption process was an endothermic reaction.

Table 1 shows the parameters from the fitting by the two isotherms models. The correlation coefficient R^2 of the Langmuir model was higher than that of the Freundlich model, indicating the Langmuir model matched better for the adsorption process (Figs. 8 and 9). According to the Langmuir model assumptions, the adsorption of $AC/Zn(OH)_2$ on MB was monolayer and uniform.

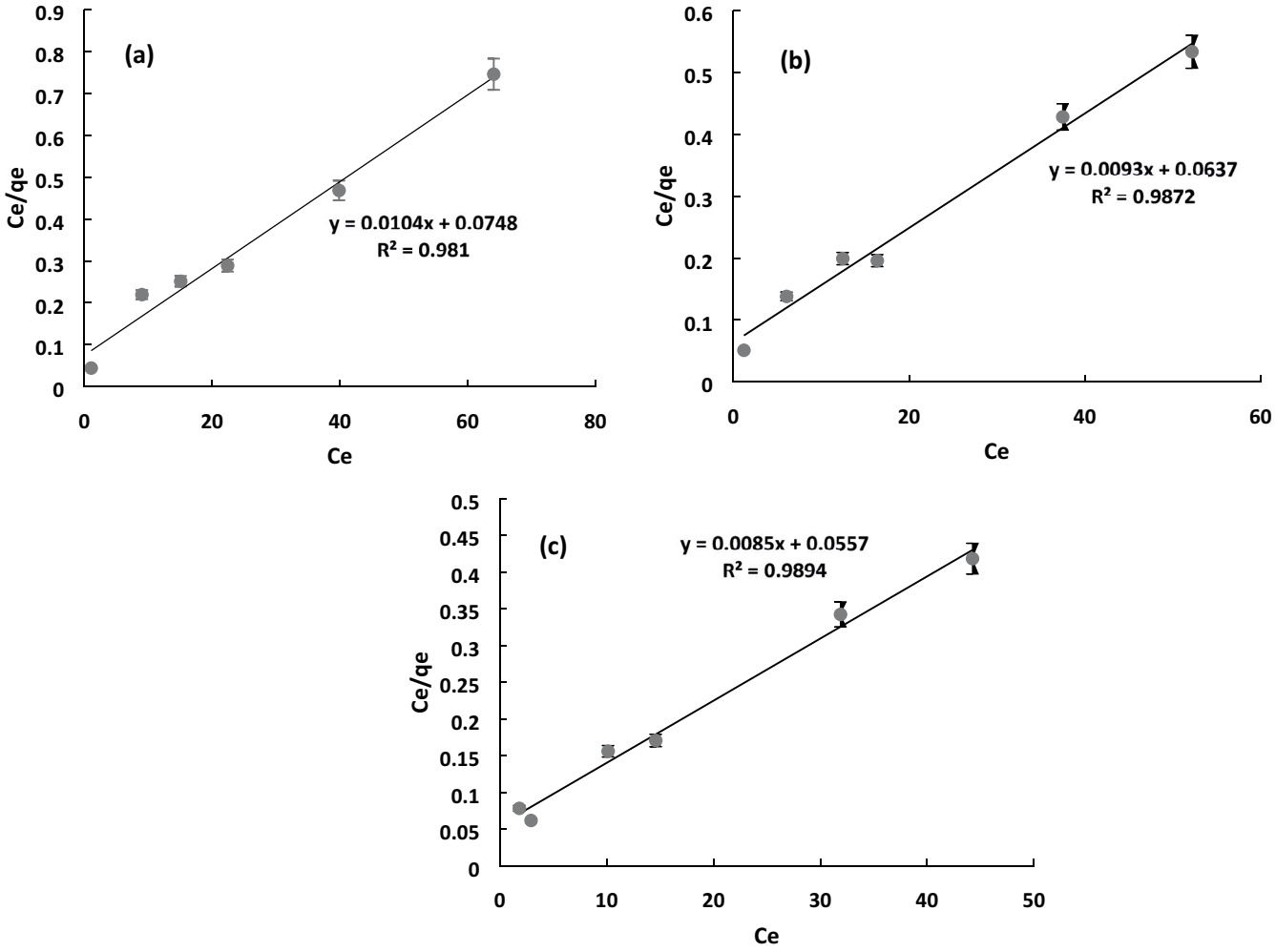

Fig. 8. Langmuir isotherm plot for the adsorption MB onto AC/$Zn(OH)_2$ composite (a) 298 K, (b) 308 K, and (c) 318 K (pH: 7; adsorbent dosage: 0.1 g; contact time: 80 min).

Table 1
Langmuir and Freundlich isotherm constants for MB adsorption

Temperature (K)	Langmuir isotherms			Freundlich isotherms		
	q_m, (mg g^{-1})	b (L mg^{-1})	R^2	K_f	n (L mg^{-1})	R^2
298	96.15	0.13	0.98	22.96	2.93	0.95
308	107.53	0.14	0.99	23.23	2.59	0.94
318	117.65	0.15	0.99	23.67	2.38	0.89

The adsorption only occurred at specific adsorption sites and MB molecules did not migrate on the AC/$Zn(OH)_2$ surface [37]. The chemical adsorption dominated the adsorption process [45], and the adsorbate removal rate was limited by the internal diffusion of MB molecules.

3.5. Influence of temperature on adsorption efficiency

The influence of temperature on MB removal yield was investigated for pH 7 at three different temperatures 298, 308, and 318 K in 0.1 g/100 mL dose and 100 mg L^{-1} initial MB concentration. The change of MB adsorption concerning temperature is shown in Fig. 10.

As can be seen in Fig. 10, MB removal increases with increasing temperature. Increasing the temperature leads to an increase in the diffusion rates of the dyestuff. Also, temperature increase can enhance the adsorptive interactions at higher temperatures by strengthening the bonds between the dye molecules and increasing the binding sites of the sorbent. It has been observed that the findings obtained by the temperature effect are compatible with the results of similar studies [49,50].

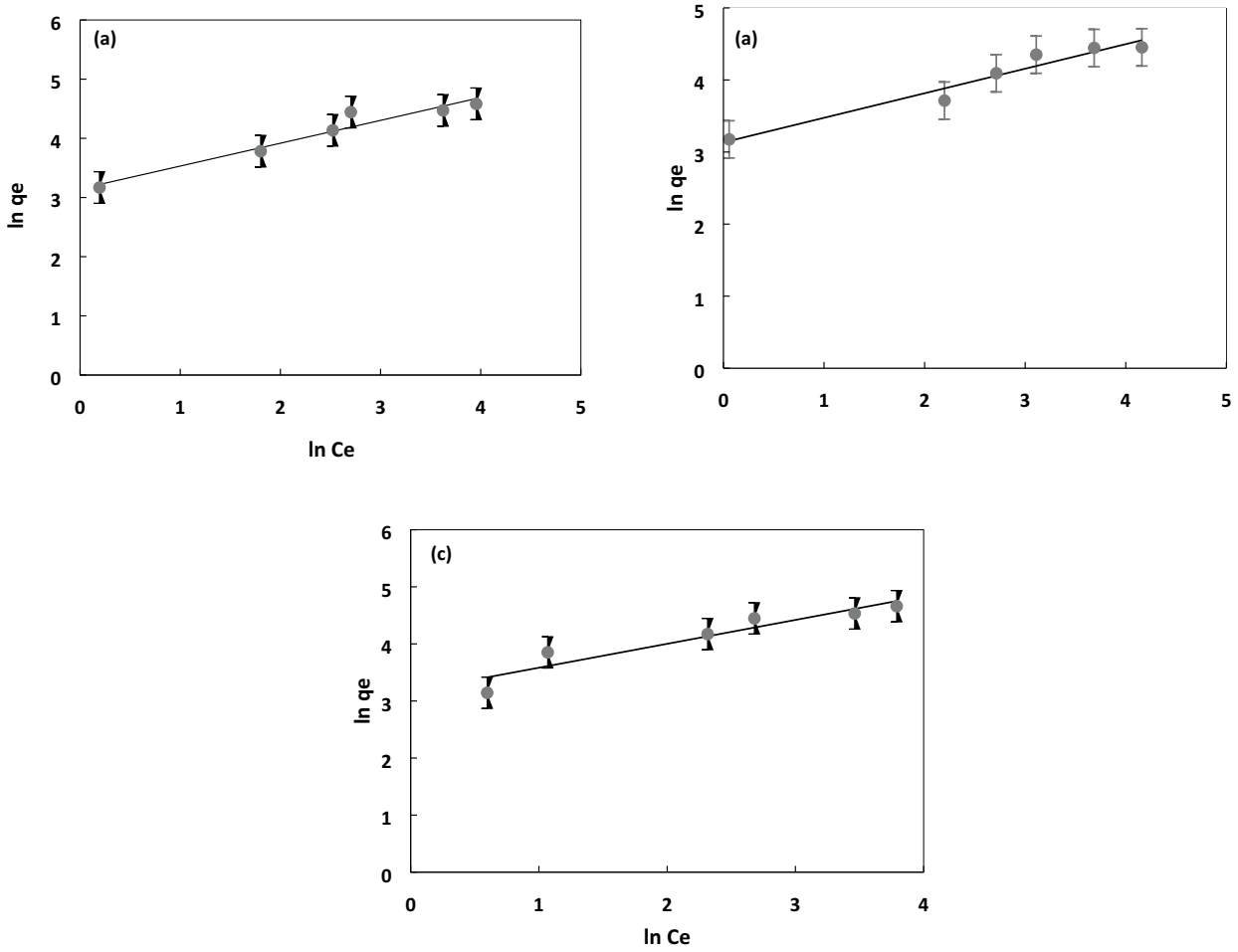

Fig. 9. Freundlich isotherm plot for the adsorption MB onto AC/$Zn(OH)_2$ composite (a) 298 K, (b) 308 K, and (c) 318 K (pH: 7; adsorbent dosage: 0.1 g; contact time: 80 min).

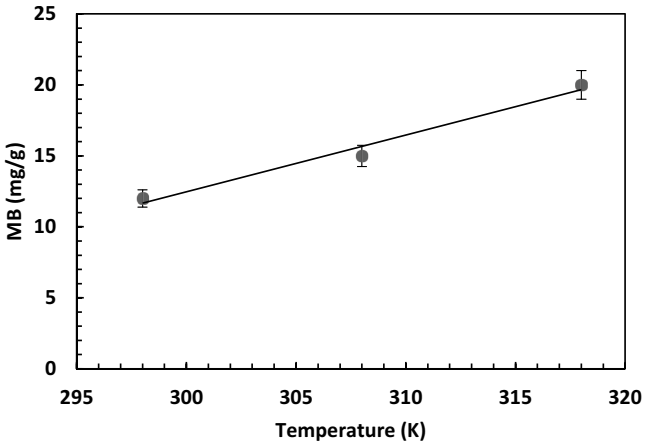

Fig. 10. Effect of temperature on the adsorption of MB (contact time: 80 min; pH: 7; adsorbent dose: 0.1 g/100 mL).

3.6. Thermodynamic study

Adsorption thermodynamics is important to understand the mechanism of the adsorption process and the effect of temperature on the adsorption process [41]. The influence of temperature on the adsorption of MB between 298 and 318 K was studied by using 0.1 g of AC/$Zn(OH)_2$ 50 mg L^{-1} MB solutions The thermodynamic parameters of Gibbs energy ($\Delta G°$), standard enthalpy ($\Delta H°$), and entropy ($\Delta S°$) can be calculated using the following Eqs. (5)–(7) [42].

$$\Delta G° = -RT\ln K_L \tag{5}$$

where R is the gas constant (8.314 J mol^{-1} K^{-1}), T is the temperature (K), and K_L is known as the distribution coefficient. The equilibrium constant (K_L) was estimated as:

$$K_L = \frac{q_e}{C_e} \tag{6}$$

According to the van't Hoff equation:

$$\ln K_L = \frac{\Delta S°}{R} - \frac{\Delta H°}{RT} \tag{7}$$

The values of $\Delta H°$ (kJ mol^{-1}) and $\Delta S°$ (J mol^{-1} K^{-1}) were evaluated from the slope and intercept of the van't Hoff

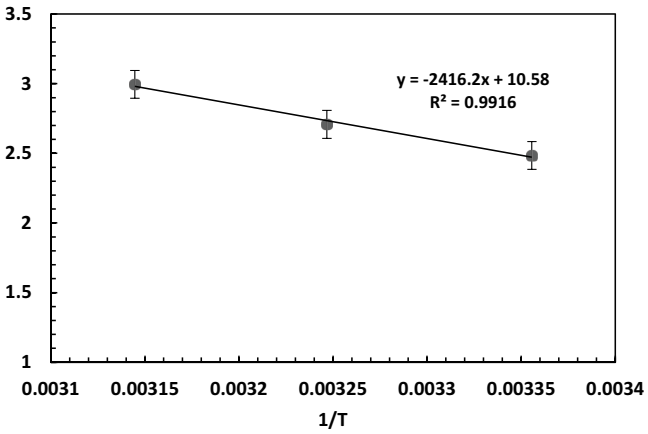

Fig. 11. van't Hoff plot for the adsorption of MB on AC/$Zn(OH)_2$ (pH: 7; adsorbent dosage: 0.1 g; contact time: 80 min).

Table 2
Thermodynamic parameters calculated for MB adsorption

T (K)	$\Delta G°$ (kJ mol^{-1})	$\Delta H°$ (kJ mol^{-1})	$\Delta S°$ (J mol^{-1})
298	–3.76	50.09	0.18
308	–5.07		
318	–7.35		

plots (Fig. 11) [50,51]. The thermodynamic parameters obtained for the adsorption of MB are shown in Table 2.

As can be seen from Table 2, the values of K_L (equilibrium constant) increased with increasing temperature. It depends on the Gibbs free energy whether the adsorption is spontaneous or not, and the presence of $\Delta G°$ as a negative indicates that the adsorption is spontaneous [40–42]. In addition, an increase in $\Delta G°$ with an increase in temperature indicates that MB is more adsorbed at high temperatures. The positive value of $\Delta S°$ showed an increase in randomness at the solid/solution interface during the adsorption of MB dye on AC/$Zn(OH)_2$. A positive $\Delta H°$ value is an indication that the adsorption is endothermic.

3.7. Adsorption kinetics

Adsorption kinetics is used to specify which mechanisms play a role during the adsorption of the adsorbed substance onto the adsorbent surface. In order to understand the kinetics behind the MB removal process, pseudo-first and pseudo-second-order models were employed to analyze the kinetic data. AC/$Zn(OH)_2$ (0.1 g) samples were conducted with 100 mL MB (25 and 50 mg L^{-1}) solutions to determine the effect of contact time on adsorption. The equations of pseudo-first-order and pseudo-second-order were shown in Eqs. (8) and (9), respectively.

The equality of pseudo-first-order equations:

$$\log\left(q_e - q_t\right) = \log q_e - k_1 t \tag{8}$$

The equality of pseudo-second-order equations:

$$\frac{t}{q_t} = \frac{1}{k_2 q_e^2} + \frac{t}{q_e} \tag{9}$$

where q_e: adsorption amounts at equilibrium (mg g^{-1}), q_t: amount of adsorbent per gram of adsorbent in any time (mg g^{-1}), t: contact time (min), k_1: pseudo-first-order speed constant (min^{-1}), k_2: pseudo-second-order speed constant (g mg^{-1} min^{-1}) [51–53]. The linearity of the kinetic model is very important in deciding which model is suitable for the adsorption system.

The kinetic parameters and correlation coefficient (R^2) values were obtained from Figs. 12 and 13 and are listed in Table 3. As a result of the data, the compatibility of the adsorption kinetic mechanism with the pseudo-second-order kinetic model was revealed as a result of the values of R^2. As a result of this, it was seen that the MB molecules hold on to the AC/$Zn(OH)_2$ molecules and there is an activation.

The proximity of experimental and theoretical q_e values is the main criterion for deciding which kinetic model defines the adsorption system. As can be seen from Table 3, in our study it was found that the experimental and theoretical q_e values of the second-order are closer than those of the first-order equation. When the pseudo-first-order kinetic model and the pseudo-second-order kinetic model were compared to the adsorbent, a higher correlation coefficient was obtained in the pseudo-second-order kinetic model. The increase in adsorption and contact time increases the resistance and mobility of the dye during adsorption. Since the uptake of MB at the active sites of AC/$Zn(OH)_2$ is a rapid process, the rate of adsorption is mainly governed by liquid phase mass transfer rate, diffusion through the boundary layer, or intra-particle mass transfer rate. The high agreement obtained shows the strong interaction between the functional groups on AC/$Zn(OH)_2$ and the MB molecules. There are similar results in many studies on MB adsorption in the literature [19,54,55].

Table 3
Parameters of the pseudo-first-order and the pseudo-second-order for MB adsorption

C_o (mg L^{-1})	Pseudo-first-order				Pseudo-second-order		
	$q_{e,exp}$	k_1, min^{-1}	$q_{e,cal}$ (mg g^{-1})	R^2	k_2 (g mg^{-1} min^{-1})	$q_{e,cal}$ (mg g^{-1})	R^2
25	23.16	0.017	11.11	0.73	0.099	24.81	0.99
50	47.26	0.007	8.64	0.77	0.200	48.54	0.99

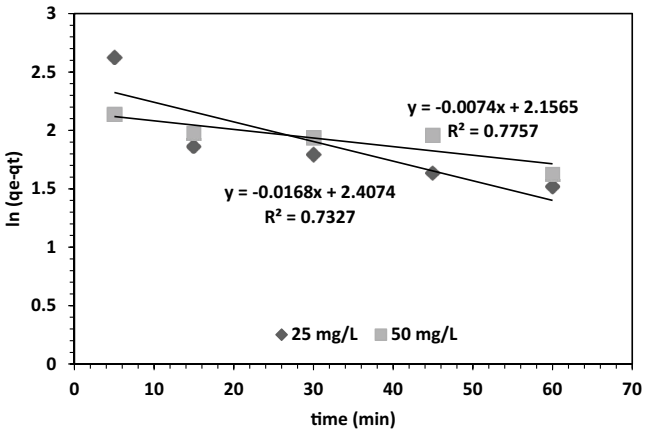

Fig. 12. Pseudo-first-order kinetic model plot of MB adsorption (adsorbent dose: 0.1 g/100 mL; pH: 7; temperature: 298 K).

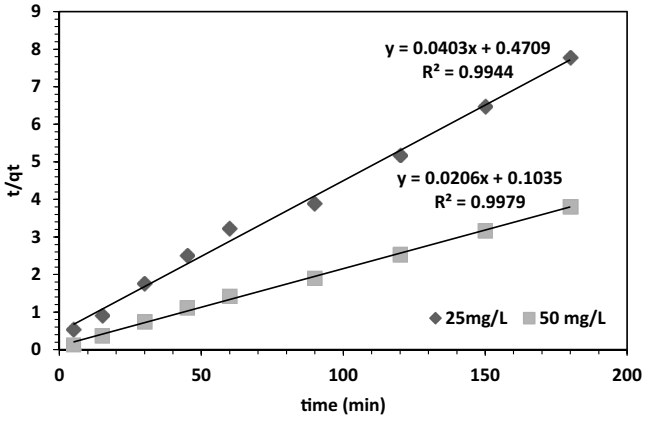

Fig. 13. Pseudo-second-order kinetic model plot of MB adsorption (adsorbent dose: 0.1 g/100 mL; pH: 7; temperature: 298 K).

3.8. Comparison of the adsorption capacity of the developed adsorbent in terms of different adsorbents

The adsorption capacity is an important parameter in dyestuff removal. In Table 4, the q_{max} values for the removal of MB using the AC/$Zn(OH)_2$ adsorbent were compared with different types of adsorbents in the literature [38,45,56–59].

The maximum adsorption capacity of the AC/$Zn(OH)_2$ was compared with some other adsorbents reported in the literature as shown in Table 4. As can be seen from Table 4, compared to AC/$Zn(OH)_2$ and other different adsorbents, the proposed method and adsorption capacity for AC/$Zn(OH)_2$ are preferable and shows satisfactory removal for MB. When compared with the studies in the literature, it was observed that the amount of adsorbent was generally chosen between 0.01–2.0 g mL^{-1}. In our study, we chose an adsorbent dose of 0.1 g, as removal efficiency was achieved above 95%. When compared with the studies in the literature, it was observed that the adsorption capacity was generally between 15.49–269.3 mg g^{-1}. It was observed that the adsorption capacities of AC/$Zn(OH)_2$ were found to be 117.65 mg g^{-1}. According to this, it shows that AC/$Zn(OH)_2$ adsorbent has an effective adsorption capacity in removing MB from aqueous solutions.

4. Conclusion

The primary objective of this study is to produce acorn shell-based AC as a novel, abundantly available, low-budget, environmentally friendly new adsorbent by modifying it with the use of ultrasonic cavitation using $Zn(OH)_2$. The bio-based AC was doped ultrasonically with $Zn(OH)_2$ and used successfully for the removal of MB from an aqueous solution. As a result of these studies, it has been shown that pH, temperature, adsorbent dosage, and initial MB concentration have a significant impact on the adsorption process. For maximum removal the optimum pH was found to be 7, the contact time was 80 min, the amount of adsorbent was 0.1 g, and the temperature was 318 K. The Langmuir equation was found to have a high degree of applicability to the experimental data obtained in this work. This occurs in a single layer involving electrostatic attraction forces. This occurs in a single layer involving electrostatic attraction forces. According to the Langmuir adsorption isotherm, the highest adsorption capacity was found to be 117.65 mg g^{-1} at 318 K as a result of calculations for the adsorption of MB dyestuff on AC/$Zn(OH)_2$. The kinetic studies have shown that the pseudo-second-order model is particularly compatible when it comes to identifying the adsorption mechanism for AC/$Zn(OH)_2$. Thermodynamic calculations showed that the MB adsorption was endothermic and spontaneous. The results obtained from the study support the view that

Table 4
Comparison of MB adsorption capacities of different adsorbents in the literature

Adsorbent	pH	Temperature (K)	Dosage (g mL^{-1})	C_o (mg L^{-1})	Adsorption capacity (mg g^{-1})	References
$Zn(OH)_2$-NPs-AC from cherry tree	6.0	298	0.025/100	12.5	41.49	[38]
CuO nanoparticles loaded on AC	7.0	298	–	–	15.49	[45]
Rectorite/Fe_3O_4/ZnO	6.0	298	0.9/100	5.0	35.1	[56]
Euphorbia rigida-based AC	6.0	313	2/100	100–400	114.5	[57]
Cocos nucifera L.	8.0	298	0.1/100	250	15.775	[58]
Dipterocarpus alatus fruit AC	6–6.5	298	0.01	6–450	269.3	[59]
AC/$Zn(OH)_2$	7.0	298	0.1/100	25–150	117.65	This study

synthesized AC/$Zn(OH)_2$ has the potential to act as an alternative adsorbent for the successful removal of MB from aqueous solutions.

References

[1] S. Shoukat, H.N. Bhatti, M. Iqbal, S. Noreen, Mango stone biocomposite preparation and application for crystal violet adsorption: a mechanistic study, Microporous Mesoporous Mater., 239 (2017) 180–189.

[2] H. Shayesteh, A. Ashrafi, A. Rahbar-Kelishami, Evaluation of Fe_3O_4@MnO_2 core-shell magnetic nanoparticles as an adsorbent for decolorization of methylene blue dye in contaminated water: synthesis and characterization, kinetic, equilibrium, and thermodynamic studies, J. Mol. Struct., 1149 (2017) 199–205.

[3] A.H. Jawad, A.S. Abdulhameed, A. Reghioua, Z.M. Yaseen, Zwitterion composite chitosan-epichlorohydrin/zeolite for adsorption of methylene blue and reactive red 120 dyes, Int. J. Biol. Macromol., 163 (2020) 756–765.

[4] C. Djelloul, A. Hasseine, Ultrasound-assisted removal of methylene blue from aqueous solution by milk thistle seed, Desal. Water Treat., 51 (2013) 28–30.

[5] P. Sharma, S. Pandey, Status of phytoremediation in world scenario, Int. J. Environ. Biorem. Biodegrad., 2 (2014) 178–191.

[6] K.T. Chung, Azo dyes and human health: a review, J. Environ. Sci. Health., Part C Environ. Carcinog. Ecotoxicol. Rev., 34 (2016) 233–261.

[7] L. Bianco, E. D'Amico, A. Villone, F. Nanna, D. Barisano, Bioremediation of wastewater stream from syngas cleaning via wet scrubbing, Chem. Eng. Trans., 80 (2020) 31–36.

[8] D. Rajkumar, B.J. Song, J.G. Kim, Electrochemical degradation of Reactive Blue 19 in chloride medium for the treatment of textile dyeing wastewater with identification of intermediate compounds, Dyes Pigm., 72 (2017) 1–7.

[9] S. Meric, D. Kaptan, T. Olmez, Color and COD removal from wastewater containing Reactive Black 5 using Fenton's oxidation process, Chemosphere, 54 (2004) 435–441.

[10] J. Joseph, R.C. Radhakrishnan, J.K. Johnson, S.P. Joy, J. Thomas, Ion-exchange mediated removal of cationic dye-stuffs from water using ammonium phosphomolybdate, Mater. Chem. Phys., 242 (2020) 1–8.

[11] M.H. Dehghani, P. Mahdavi, Removal of acid 4092 dye from aqueous solution by zinc oxide nanoparticles and ultraviolet irradiation, Desal. Water Treat., 54 (2015) 3464–3469.

[12] T. El Malah, H.F. Nour, E.K. Radwan, R.E. Abdel Mageid, T.A. Khattab, M.A. Olson, A bipyridinium-based polyhydrazone adsorbent that exhibits ultrahigh adsorption capacity for the anionic azo dye, Direct Blue 71, Chem. Eng. J., 409 (2021) 128195, doi: 10.1016/j.cej.2020.128195.

[13] M.M. El Bendary, E.K. Radwan, M.F. El-Shahat, Valorization of secondary resources into silica-based adsorbents: preparation, characterization and application in dye removal from wastewater, Environ. Nanotechnol. Monit. Manage., 15 (2021) 100455, doi: 10.1016/j.enmm.2021.100455.

[14] A.A. Alqadami, M.A. Khan, M.R. Siddiqui, Z.A. Alothman, Development of citric anhydride anchored mesoporous MOF through post synthesis modification to sequester potentially toxic lead(II) from water, Microporous Mesoporous Mater., 261 (2018) 198–206.

[15] R.C. Bansal, M. Goyal, Activated Carbon Adsorption, CRC Press, Taylor and Francis, London, 2005.

[16] A.M. Puziy, O.I. Poddubnaya, A. Martínez-Alonso, F. Suárez-García, J.M.D. Tascón, Surface chemistry of phosphorus-containing carbons of lignocellulosic origin, Carbon, 43 (2005) 2857–2868.

[17] A.M. Puziy, O.I. Poddubnaya, A. Martínez-Alonso, F. Suárez-García, J.M.D. Tascón, Synthetic carbons activated with phosphoric acid: I. Surface chemistry and ion binding properties, Carbon, 40 (2002) 1493–1505.

[18] E.K. Radwan, S.T. El-Wakeel, T.A. Gad-Allah, Effects of activation conditions on the structural and adsorption characteristics of pinecones derived activated carbons, J. Dispersion Sci. Technol., 40 (2019) 140–151.

[19] S. Gunes, D. Angin, Kinetic, isotherm, and thermodynamic studies of Reactive Orange 13 adsorption onto activated carbon obtained from orange pulp, Desal. Water Treat., 214 (2021) 420–432.

[20] I. Lupul, J. Yperman, R. Carleer, G. Gryglewicz, Tailoring of porous texture of hemp stem-based activated carbon produced by phosphoric acid activation in steam atmosphere, J. Porous Mater., 22 (2015) 283–289.

[21] D. Zhang, W. Cheng, J. Ma, R. Li, Influence of activated carbon in zeolite X/activated carbon composites on CH_4/N_2 adsorption separation ability, Adsorption, 22 (2016) 1129–1135.

[22] L. Khezami, R. Capart, Removal of chromium(VI) from aqueous solution by activated carbons: kinetic and equilibrium studies, J. Hazard. Mater. B, 123 (2005) 223–231.

[23] G.X. Yang, H. Jiang, Amino modification of biochar for enhanced adsorption of copper ions from synthetic wastewater, Water Res., 48 (2014) 396–405.

[24] M. Imamoglu, O. Tekir, Removal of copper(II) and lead(II) ions from aqueous solutions by adsorption on activated carbon from a new precursor hazelnut husks, Desalination, 228 (2008) 108–113.

[25] E. Altıntıg, H. Altundag, O. Ozyıldırım, I. Acar, Production of activation carbon from rice husk to support Zn^{+2} ions, Fresenius Environ. Bull., 24 (2015) 1–7.

[26] H. Nourmoradi, K.F. Moghadam, A. Jafari, B. Kamarehie, Removal of acetaminophen and ibuprofen from aqueous solutions by activated carbon derived from *Quercus Brantii* (Oak) acorn as a low-cost biosorbent, J. Environ. Chem. Eng., 6 (2018) 6807–6815.

[27] D. Angin, Production and characterization of activated carbon from sour cherry stones by zinc chloride, Fuel, 115 (2014) 804–811.

[28] M. Carrier, A.G. Hardie, U. Uras, J. Görgens, J.H. Knoetze, Production of char from vacuum pyrolysis of South-African sugar cane bagasse and its characterization as activated carbon and biochar, J. Anal. Appl. Pyrolysis, 96 (2012) 24–32.

[29] A. Kumar, H. Gupta, Activated carbon from sawdust for naphthalene removal from contaminated water, Environ. Technol. Innovation, 20 (2020) 101080, doi: 10.1016/j.eti.2020.101080.

[30] E. Flippo, A. Serra, A. Buccolieri, D. Manno, Green synthesis of silver nanoparticles with sucrose and maltose: morphological and structural characterization, J. Non-Cryst. Solids, 356 (2010) 344–350.

[31] M. Ghaedi, A. Ansari, M.H. Habibi, A.R. Asghari, Removal of malachite green from aqueous solution by zinc oxide nanoparticle loaded on activated carbon: kinetics and isotherm study, J. Ind. Eng. Chem., 20 (2014) 17–28.

[32] A. Bée, D. Talbot, S. Abramson, V. Dupuis, Magnetic alginate beads for Pb(II) ions removal from wastewater, J. Colloid Interface Sci., 362 (2011) 486–492.

[33] K.D. Hristovski, P.K. Westerhoff, T. Möller, P. Sylvester, Effect of synthesis conditions on nano-iron (hydr)oxide impregnated granulated activated carbon, Chem. Eng. J., 146 (2009) 237–243.

[34] X. Qu, P.J.J. Alvarez, Q. Li, Applications of nanotechnology in water and wastewater treatment, Water Res., 47 (2013) 3931–3946.

[35] P. Xu, G.M. Zeng, D.L. Huang, C.L. Feng, S. Hu, M.H. Zhao, C. Lai, Z. Wei, C. Huang, G.X. Xie, Use of iron oxide nanomaterials in wastewater treatment: a review, Sci. Total Environ., 424 (2012) 1–10.

[36] G. Jing, Z. Zhou, L. Song, M. Dong, Ultrasound enhanced adsorption and desorption of chromium(VI) on activated carbon and polymeric resin, Desalination, 279 (2011) 423–427.

[37] M. Breitbach, D. Bathen, Influence of ultrasound on adsorption processes, Ultrason. Sonochem., 8 (2001) 277–283.

[38] P.S. Ardekani, H. Karimi, M. Ghaedi, A. Asfaram, M.K. Purkait, Ultrasonic assisted removal of methylene blue on ultrasonically synthesized zinc hydroxide nanoparticles on activated carbon prepared from wood of cherry tree: experimental design

methodology and artificial neural network, J. Mol. Liq., 229 (2017) 114–124.
[39] Z.A. Alothman, A.H. Bahkali, M.A. Khiyami, S.M. Alfadul, S.M. Wabaidura, M. Alam, B.Z. Alfarhan, Low cost biosorbents from fungi for heavy metals removal from wastewater, Sep. Sci. Technol., 55 (2020) 1766–1775.
[40] H. Deng, G. Li, H. Yang, J. Tang, Preparation of activated carbons from cotton stalk by microwave assisted KOH and K_2CO_3 activation, Chem. Eng. J., 163 (2010) 373–381.
[41] G. Xiong, U. Pal, J.G. Serrano, K.B. Ucer, R.T. Williams, Photoluminescence and FTIR study of ZnO nanoparticles: the impurity and defect perspective, Phys. Status Solidi, 3 (2006) 3577–3581.
[42] E. Kenawy, A.A. Ghfar, S.M. Wabaidur, M.A. Khan, M.R. Siddiqui, Z.A. Alothman, A.A. Alqadami, M. Hamid, Cetyltrimethylammonium bromide intercalated and branched polyhydroxystyrene functionalized montmorillonite clay to sequester cationic dyes, J. Environ. Manage., 219 (2018) 285–293.
[43] T.H. Liou, S.J. Wu, Characteristic of microporous/mesoporous carbons prepared from rice husk under base and acid treated conditions, J. Hazard. Mater., 171 (2009) 693–703.
[44] S. Karnjanakom, P. Maneechakr, Adsorption behaviors and capacities of Cr(VI) onto environmentally activated carbon modified by cationic (HDTMA and DDAB) surfactants, J. Mol. Struct., 1186 (2019) 80–90.
[45] M. Ghaedi, A.M. Ghaedi, M. Hossainpour, A. Ansari, M.H. Habibi, A.R. Asghari, Least square-support vector (LS-SVM) method for modeling of methylene blue dye adsorption using copper oxide loaded on activated carbon: kinetic and isotherm study, J. Ind. Eng. Chem., 20 (2014) 1641–1649.
[46] H.F. Nour, R.E. Abdel Mageid, E.K. Radwan, T.A. Khattab, M.A. Olson, T. El Malah, Adsorption isotherms and kinetic studies for the removal of toxic reactive dyestuffs from contaminated water using a viologen-based covalent polymer, New J. Chem., 45 (2021) 18983–18993.
[47] T.I. Shaheen, E.K. Radwan, S.T. El-Wakee, Unary and binary adsorption of anionic dye and toxic metal from wastewater using 3-aminopropyltriethoxysilane functionalized porous cellulose acetate microspheres, Microporous Mesoporous Mater., 338 (2022) 111996, doi: 10.1016/j.micromeso.2022.111996.
[48] P.S. Kumar, P.S. Anne Fernando, R.T. Ahmed, R. Srinath, M. Priyadharshini, A.M. Vignesh, A. Thanjiappan, Effect of temperature on the adsorption of methylene blue dye onto sulfuric acid–treated orange peel, Chem. Eng. Commun., 201 (2014) 1526–1547.
[49] N. Kaya, Z. Yıldız, S. Ceylan, Preparation and characterisation of biochar from hazelnut shell and its adsorption properties for methylene blue dye, J. Polytechnic., 21 (2018) 765–776.
[50] C.J. Luk, J. Yip, C.M. Yuen, C. Kan, K. Lam, A comprehensive study on adsorption behaviour of direct, reactive and acid dyes on crosslinked and non-crosslinked chitosan beads, J. Fiber Bioeng. Inf., 7 (2014) 35–52.
[51] Mu. Naushad, A.A. Alqadami, Z.A. AlOthman, I.H. Alsohaimi, M.S. Algamdi, A.M. Aldawsari, Adsorption kinetics, isotherm and reusability studies for the removal of cationic dye from aqueous medium using arginine modified activated carbon, J. Mol. Liq., 293 (2019) 111442, doi: 10.1016/j.molliq.2019.111442.
[52] M.A. Tahir, H.N. Bhatti, M.J. Iqbal, Solar Red and Brittle Blue direct dyes adsorption onto *Eucalyptus angophoroides* bark: equilibrium, kinetics and thermodynamic studies, Environ. Chem. Eng., 4 (2016) 2431–2439.
[53] E. Altintig, A. Alsancak, H. Karaca, D. Angın, H. Altundag, The comparison of natural and magnetically modified zeolites as an adsorbent in methyl violet removal from aqueous solutions, Chem. Eng. Commun., 209 (2022) 555–569.
[54] Z.A. Al-Anber, M.A. Al-Anber, M. Matouq, O. Al-Ayed, N.M. Omari, Defatted Jojoba for the removal of methylene blue from aqueous solution: thermodynamic and kinetic studies, Desalination, 276 (2011) 169–174.
[55] H. Cherifi, B. Fatih, H. Salah, Kinetic studies on the adsorption of methylene blue onto vegetal fiber activated carbons, Appl. Surf. Sci., 282 (2013) 52–59.
[56] H. Wang, P. Zhou, R. Guo, Y. Wang, H. Zhan, Y. Yuan, Synthesis of rectorite/Fe_3O_4/ZnO composites and their application for the removal of methylene blue dye, Catalysts, 8 (2018) 1–18.
[57] O. Cercel, A. Ozcan, H.F. Gercel, Preparation of activated carbon from renewable bio-plant of *Eupharbia rigida* by H_2SO_4 activation and its adsorption behavior in aqueous solutions, Appl. Surf. Sci., 253 (2007) 4843–4852.
[58] R.H. Khuluk, A. Rahmat, Buhani, Suharso, Removal of methylene blue by adsorption onto activated carbon from coconut shell (*Cocos nucifera* L.), Indones. J. Sci. Technol., 4 (2019) 229–240.
[59] C. Patawat, K. Silakate, S. Chuan-Udom, N. Supanchaiyamat, A.J. Hunt, Y. Ngernyen, Preparation of activated carbon from *Dipterocarpus alatus* fruit and its application for methylene blue adsorption, RSC Adv., 10 (2020) 21082–21091.